Geomechanics and Engineering, *Vol. 33, No. 2 (2023) 175-182*
https://doi.org/10.12989/gae.2023.33.2.175

Estimation of liquid limit of cohesive soil using video-based vibration measurement

Matthew Sands[1], Evan Hayes[1], Soonkie Nam[2] and Jinki Kim*[1]

[1]*Department of Mechanical Engineering, Georgia Southern University, Statesboro, GA, USA 30458*
[2]*Department of Civil Engineering and Construction, Georgia Southern University, Statesboro, GA, USA 30458*

(*Received November 29, 2022, Revised April 3, 2023, Accepted April 5, 2023*)

Abstract. In general, the design of structures and its construction processes are fundamentally dependent on their foundation and supporting ground. Thus, it is imperative to understand the behavior of the soil under certain stress and drainage conditions. As it is well known that certain characteristics and behaviors of soils with fines are highly dependent on water content, it is critical to accurately measure and identify the status of the soils in terms of water contents. Liquid limit is one of the important soil index properties to define such characteristics. However, liquid limit measurement can be affected by the proficiency of the operator. On the other hand, dynamic properties of soils are also necessary in many different applications and current testing methods often require special equipment in the laboratory, which is often expensive and sensitive to test conditions. In order to address these concerns and advance the state of the art, this study explores a novel method to determine the liquid limit of cohesive soil by employing video-based vibration analysis. In this research, the modal characteristics of cohesive soil columns are extracted from videos by utilizing phase-based motion estimation. By utilizing the proposed method that analyzes the optical flow in every pixel of the series of frames that effectively represents the motion of corresponding points of the soil specimen, the vibration characteristics of the entire soil specimen could be assessed in a non-contact and non-destructive manner. The experimental investigation results compared with the liquid limit determined by the standard method verify that the proposed method reliably and straightforwardly identifies the liquid limit of clay. It is envisioned that the proposed approach could be applied to measuring liquid limit of soil in practical field, entertaining its simple implementation that only requires a digital camera or even a smartphone without the need for special equipment that may be subject to the proficiency of the operator.

Keywords: cohesive soil; computer vision; kaolin clay; liquid limit; modal analysis; phase-based motion estimation; vibrations

1. Introduction

In general, the design and construction of structures as well as their stability afterward are fundamentally dependent on their foundations and supporting ground. Thus, it is significantly important to understand the behavior of the soil during and after the construction. As it is well known that certain types of soils contain more fines, and their characteristics and behaviors are highly dependent on water content (Lu 2019), it is critical to accurately measure and identify the status of the soils in terms of water contents.

Unlike coarser soils that the physical properties are mostly dependent on the particle sizes and shapes, fine soils usually change their physical properties with the changes of water content, which is known as plasticity. Its status changes from liquid to plastic and plastic to semi-solid states. Atterberg (1911) defined the corresponding limits as liquid limit (LL) and plastic limit (PL) respectively, which are usually determined by laboratory experiments. The Atterberg limits help engineers evaluate the plasticity and consistency of soils with fines at different water contents.

These limits are very useful to characterize, classify, and predict the engineering behavior of fine soils (Polidori 2007). Thus, they are usually considered as fundamental properties of soils and indicators to show the effectiveness of soil improvement, which can be correlated with other engineering properties (Yasodian *et al.* 2012).

When determining the liquid limit which is one of the soil index properties to define consistency of fine soils, there are two widely accepted test methods: the Casagrande's method using a percussion cup (also known as Casagrande cup) and the fall cone method using a small falling cone (also known as cone penetrometer). The Casagrande cup device was developed by Casagrande (1932, 1958) and is favored in the U.S. (AASHTO 2013, ASTM 2005) although it is also included in the British Standards (BS) (British Standards Institute 2022). On the other hand, the fall cone method is known to be more popular in Europe and Asia, and is adopted in the BS and International Organization for Standardization (ISO) Standards (British Standards Institute 2022, Coduto *et al.* 2011, ISO 2022). Even though the standards describe the specific requirements for the testing devices and procedures, some researchers have noticed inconsistency between two methods and tried to correlate each other (Di Matteo 2012, Shimobe and Spagnoli 2019). Furthermore, a

*Corresponding author, Assistant Professor
E-mail: jinkikim@georgiasouthern.edu

ISSN: 2005-307X (Print), 2092-6219 (Online)

certain consistency is required in the standards as the results can be affected by the proficiency of the operator (ASTM 2005), and the devices and operator's skill may influence the reliability and reproducibility of the test results. While novel approaches utilizing devices and technologies such as visible near-infrared spectroscopy have recently been proposed (Knadel *et al*. 2021, Rehman *et al.* 2019), these approaches require relatively expensive and sophisticated equipment to estimate the liquid limit in a laboratory setting.

In order to address this concern and advance the state of the art, this research explores a novel non-contact and non-destructive method that can reliably determine the liquid limit of cohesive soil by monitoring the vibration characteristics of soil samples extracted from videos via phase-based motion estimation (Wadhwa *et al.* 2013). The key principle of the proposed method is based on a hypothesis that the soil may lose elastic stability and thus its natural frequency may approach zero as the water content level approaches the liquid limit. The proposed approach yields a straightforward implementation that requires only a digital camera without the need for special equipment, which is not dependent on the proficiency of the operator as well. In the following sections, the proposed experimental method for measuring the vibration characteristics and estimating the liquid limit of cohesive soil samples is first presented. Next, experimental investigation results are presented to validate the effectiveness of the proposed approach. Finally, concluding remarks are provided to summarize the findings and reflect on the potential of the new approach.

2. Materials and method

2.1 Kaolin clay and sample preparation

To evaluate the elastic modulus and liquid limit of cohesive soil, kaolin clay was chosen to fabricate cylindrical samples, since it is one of the representative clayey soils that has been widely employed in various experimental studies to identify certain characteristic of fine soils (e.g., Alrubaye Ali *et al*. 2018, Bore *et al*. 2021, Çakar and Yukselen-Aksoy 2021, Lee and Shang 2011). A commercially available kaolin clay is used for the study.

The clay is tested according to the ASTM standards (ASTM 2000; ASTM 2005; ASTM 2010; ASTM 2017) and its liquid limit (LL), plastic limit (PL), specific gravity (G_s), fine contents, and classification by the Unified Soil Classification System (USCS) are determined as shown in Table 1.

In order to obtain reference values of liquid limit of the kaolin clay, a series of liquid limit tests using the Casagrande apparatus is performed following the standard multipoint method in ASTM D 4318 (ASTM 2005) and the results are shown in Fig. 1.

Kaolin clay pastes with moisture contents ranging from 32% to 40% are fabricated by adding different amounts of water with the kaolin clay powder in a dry state. The pastes are hand-mixed using a spatula to achieve a homogeneous

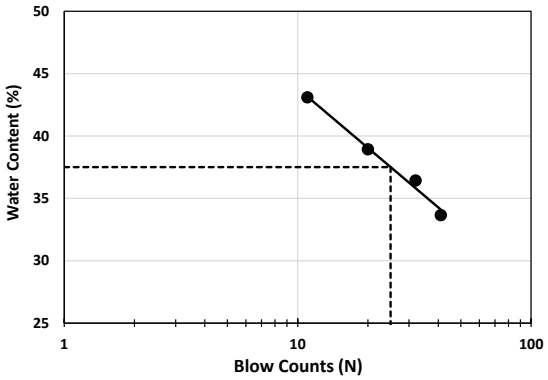

Fig. 1 Liquid limit test results using Casagrande apparatus

Table 1 Property of Kaolin clay

	LL	PL	G_s	Passing #200 sieve (<75 μm)	USCS
Kaolin clay	37.5	17	2.61	100%	CL

mixture. The clay mixture was then formed into cylindrical samples by compressing the mixture into a cylindrical mold, where the height (L) is 53.3 mm and the diameter (d) is 17.5 mm. These dimensions were selected as they mitigate the influence of gravity by keeping the effective stiffness high enough such that the samples do not collapse upon themselves. In the case of a very soft soil (high water content), the sample may collapse upon itself, negatively impacting measurement. In the case of a stiffer soil (very low water content), the structure may resonate at a higher frequency, requiring the dimensions of the sample to be modified such that the sample's resonant frequency remains low enough for it to be measured by a relatively low sampling rate. In practical applications, sample dimensions may be adjusted on the fly in the event of a low moisture soil (requiring larger dimensions) or high moisture soil (requiring smaller dimensions). The samples are then gently extruded out of the mold using a special plunger to create clay columns preserving their regular shape. Three samples are fabricated for each moisture content. The weight of each sample is measured by a digital balance to obtain the unit weight, and moisture content is measured after the tests to verify the consistency of the samples.

2.2 Dynamic testing setup

Fig. 2 illustrates the experimental setup used in this study to validate the effectiveness of the proposed method by measuring the dynamic response of the clay columns. The clay column is fixed to a linear roller slide (#4301, Parker) by adhesive film. The slide is capable of moving only in a single linear direction. The slide is controlled by a stepping motor (17HS4401, Usongshine) linked to the base by a connecting arm, such that the motor's rotation is converted to lateral motion. By connecting the stepping motor that provides a rotational output to the slider via a connecting arm, the rotation of the motor may be converted to a linear horizontal motion. A consistent lateral impulse is

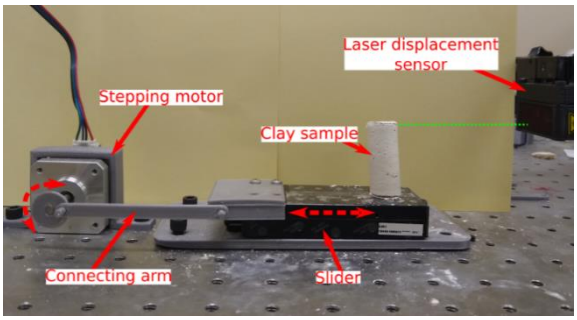

Fig. 2 Experimental setup to provide an impulsive base excitation to the clay sample and measure its dynamic behavior for estimating the liquid limit

provided by sliding the base at velocity of approximately 0.3 m/s and abruptly stopping. This is realized via Arduino controller programmed to allow the stepping motor to rotate for a set amount of time before stopping the motor. The base is accelerated for about 15 mm and comes to an abrupt stop, so that the clay sample undergoes a base impulse with a peak acceleration of approximately 20 m/s^2, measured by an accelerometer (352C22, PCB Piezotronics).

The displacement of the clay columns when subjected to an impulsive base excitation is simultaneously measured by a laser displacement sensor (optoNCDT 1420, Micro-Epsilon) at a sampling rate of 4000 Hz and a 1.3 megapixel (1280×1024 CMOS sensor) camera (Chronos 1.4, Kron Technologies) equipped with a 12.5 - 75 mm f/1.2 zoom lens. Resolution (768 × 940 pixels) and frame rate (250 frames per second) for the video are selected to record as much of the structure's spatiotemporal data as possible. Displacement is captured from the time of the initial impulse until the clay sample settles, approximately 1 second after the impulse. The distance between the camera and the clay sample was approximately 300 mm to capture the sample's full oscillation within the field of view of the camera. The camera is fixed to a tripod to mitigate noise induced by ambient vibrations.

It is worth noting that while ambient vibrations may be a possible source to introduce unwanted noise, the proposed method is capable of reliably and straightforwardly identifying the liquid limit of kaolin clay in the field due to its relatively simple and compact apparatus. The testing apparatus may be easily repositioned to the best suited area for measurement. For example, the apparatus may be carried inside of a small bag and deployed directly on to the ground, which is often rigid enough to mitigate ambient noise to the high frequency domain. Additionally, the motion induced by holding the camera may be easily mitigated by mounting to a tripod. Furthermore, the impulsive base excitation (approximately 20 m/s^2 in this study, which can also be adjusted as needed) provided by the proposed apparatus generates significant motion compared to that induced by ambient excitation noise.

2.3 Phase-based motion estimation

The experimentally obtained video measurement is then processed utilizing phase-based motion estimation

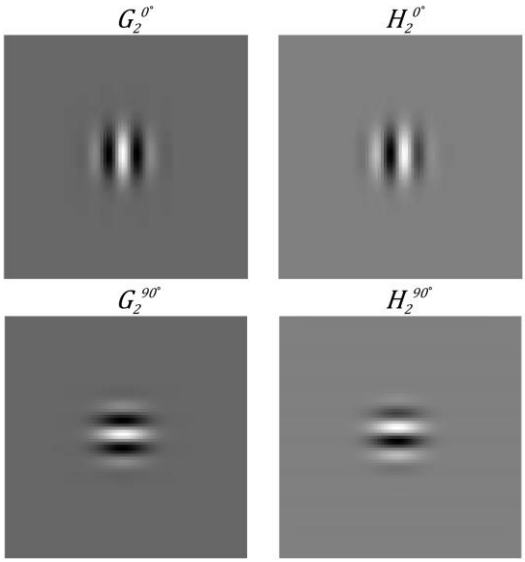

Fig. 3 The real and imaginary parts of 2D Gabor wavelets for orientations 0° and 90°, which filter horizontal and vertical motion, respectively. The gray level corresponds to the filter's magnitude

(Chen *et al.* 2015, Kim *et al.* 2022, Wadhwa *et al.* 2013), an algorithm that relates the phase shift of the pixel intensity in the frequency domain to displacement captured through video. However, since the sinusoidal basis function of the Fourier transform used to obtain the frequency response is spatially global, the Fourier transform can only handle global motions in the video. This is overcome by employing complex steerable pyramid filters $G_2^\theta + iH_2^\theta$ (Simoncelli and Freeman 1995), allowing for the video to be decomposed into local amplitude $A_\theta(x,y,t)$ and local phase $\phi_\theta(x,y,t)$ at location (x,y) and time t by spatially bandpassing each frame with pixel intensity $I(x,y,t)$.

$$\left(G_2^\theta + iH_2^\theta\right) \otimes I(x,y,t) = A_\theta(x,y,t)e^{i\phi_\theta(x,y,t)}, \quad (1)$$

where G_2^θ and H_2^θ are the real and imaginary parts of the complex filter for orientation θ, and $\otimes$ represents convolution operation. Fig. 3 serves to illustrate the magnitude of the filters on a gray level, which are based on a 9 by 9 grid of numbers. The coefficients used to compute the horizontal and vertical local phase and amplitude are provided in Table A1 in the Appendix. 2D Gabor wavelet filters (Chen *et al.* 2015) with orientations 0° and 90° are utilized in this study as a basis function for the localized Fourier transform such that local phase shifts in the horizontal and vertical directions of the video may be obtained and related to displacement. For each pixel within the image sequence, the local phase over time is filtered using a Tukey window with a cosine/constant section ratio of 0.1 for leakage protection with fair amplitude accuracy. Since motion is based on intensity changes in each pixel of the video, displacement is only extracted in areas with high contrast. Low contrast areas are masked out to reduce noise in the spectral domain.

The frequency response of the clay columns is obtained by performing a fast-Fourier transform on the individual

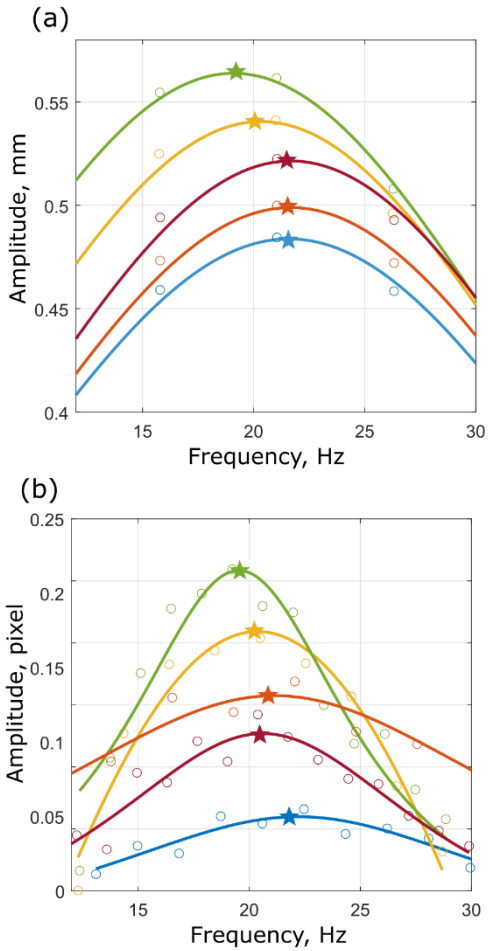

Fig. 4 Frequency responses near the fundamental resonance frequency for flexural vibrations, which are obtained by (a) laser-based and (b) video-based methods. Solid curves indicate Lorentzian fit to experimental data (circles). The resonance frequencies identified by the peaks are indicated by stars

filtered signals of each pixel and averaging in the frequency domain. From the frequency spectrum, areas of local maxima, or "peaks" in the signal are considered as areas encompassing resonant frequencies. Areas with no peaks in the signal are masked from the frequency spectrum. The areas including peaks are then fitted to a Lorentzian distribution to mitigate error due to frequency resolution. From the fitted signal, the resonant frequencies may be easily determined by identifying the frequency at the peak.

Once the resonance frequencies are identified from the frequency response, phase-based motion magnification (Wadhwa *et al.* 2013) is employed to identify their corresponding mode shapes. The video measurement is bandpass filtered near the resonance frequencies of interest and multiplied by an amplification factor to magnify the motion. Then the video is reconstructed in the time domain to realize the magnified video that corresponds to operational deflection shape near the vibration mode. The amplification factor is manually selected such that the mode shape may be easily identified while minimizing noise and magnification artifacts. A detailed explanation of this method can be found in the literature (Wadhwa *et al.* 2013).

Table 2 Mean and standard deviation values of fundamental resonant frequencies of a single clay sample (34% water content) measured five times

	Trial 1	Trial 2	Trial 3	Trial 4	Trial 5	Mean	Standard deviation
Laser-based measurement, Hz	21.6	20.2	19.0	21.7	21.1	20.7	1.1
Video-based measurement, Hz	22.2	20.4	19.6	20.6	21.2	20.8	0.99

3. Results and discussion

3.1 Effectiveness of video-based vibrometry for clay measurement

To evaluate the effectiveness and reliability of the proposed video-based method for estimating elastic parameters and liquid limit of cohesive soil, the fundamental resonance frequency of the flexural mode for a clay column with 34% water concentration is measured simultaneously by laser displacement sensor and camera five times.

The spectral amplitudes around the fundamental resonance frequency of the clay specimen, which is obtained by utilizing the laser- and video-based vibrometry are provided in Fig. 4. The frequency responses are fitted to a Lorentzian distribution to estimate the resonance frequency at the peak, which is applied for all experimental results analyzed in this study.

By applying a Lorentzian fit to the raw spectral response and finding the point on the horizontal axis which corresponds to the maximum amplitude of each curve in Fig. 4 (noted by stars), the resonant frequency may be estimated. The resulting resonance frequency values are documented in Table 2 with mean and standard deviations.

It is shown that both laser- and video-based approaches with the impulsive base excitation system offer high reliability with a standard deviation of 5.4% and 4.7%, respectively, between five measurements of a single clay sample. Furthermore, Table 2 presents that the resonance frequencies measured by the proposed video-based methods exhibit excellent quantitative agreement (absolute difference less than 0.3%) with those obtained by conventional laser-based approach. Overall, these results clearly support that the experimental setup using video-based approach provides reliable measurement of the vibration characteristic of the clay sample in a non-contact manner.

3.2 Experimentally estimated liquid limit

Following the experimental verification of the consistency and reliability of the proposed video-based measurement approach, the effectiveness of the proposed method is evaluated for estimating the liquid limit of

Table 3 Mean and standard deviations of the experimentally extracted resonance frequencies

Water content	32%	33%	34%	35%	36%	37%	38%	39%	40%
Mean, Hz	42.7	33.9	31.6	16.8	10.0	8.1	6.0	5.8	5.6
Standard deviation, Hz	8.4	1.8	2.5	4.0	3.5	3.5	0.1	0.2	0.3

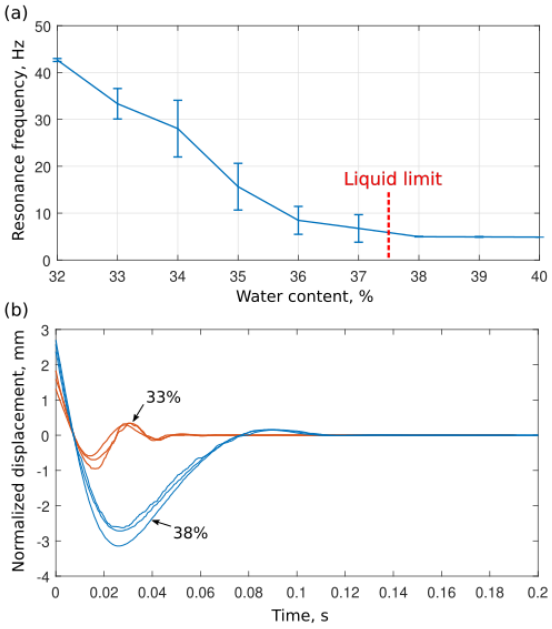

Fig. 5 (a) Experimentally obtained resonance frequency for different water content in kaolin samples. Error bars indicate one standard deviation and (b) Normalized displacements of the clay samples with 33% and 38% water content. While samples below the liquid limit (37.5%) exhibits oscillatory response, samples with high water content does not undergo significant oscillations but gradually recover to the equilibrium point

cohesive soil. In this study, three kaolin clay samples are prepared for each water content level ranging from 32% to 40%. The samples are fabricated following the procedure detailed in Sec. 2.1.

The experimentally obtained resonance frequencies of the clay samples using the proposed approach for each moisture content level are illustrated in Fig. 5(a). Table 3 documents the recorded resonance frequencies for each water content level. On average, the standard deviation of the experimentally obtained resonance frequencies resulted in 15%, which supports that the experimental setup provides reliable measurement and fabrication of the clay samples. It is clearly observed from Fig. 5(a) that the fundamental resonance frequency decreases as the water content level increases from 32% to 40%. Here, we notice that the resonance frequency dramatically decreases for water content level lower than 37% and then decreases gradually afterwards. This result shows that there appears to be a relation between the resonance frequency, water content level, and the liquid limit.

In the case of low-water content, soil sample exhibits a high effective stiffness and resonates at a relatively high frequency with more significant oscillation, as illustrated in Fig. 5(b). On the other hand, as water content increases, soil becomes more of a soft structure, leading to lower effective stiffness and resonance frequency. Samples below 38% also exhibit oscillatory response when impulsive base excitation was applied, illustrated in Fig. 5(b) as an example. However, the samples with water content level higher than 38% did not exhibit significant oscillations but gradually recovered to the equilibrium point. This provides great quantitative agreement with the liquid limit (37.5%) experimentally determined by the Casagrande cup method (ASTM 2005), shown in Fig. 1. This mechanical behavior may be attributed to the decrease in the elastic modulus of clay with higher moisture content and transition to the liquid state. As a result, the liquid limit may be straightforwardly estimated by monitoring the resonance frequency changes of clay samples depending on water content level in a non-contact manner.

It is worth noting that the proposed approach also alleviates the issue that traditional liquid limit measurement methods are highly dependent on the proficiency of the operator, by providing an objective excitation, measurement, and analysis methodology. Furthermore, the proposed vibration-based method is relatively easy to adapt to and comes without the need for special equipment, only requiring an electric motor, bearing-based slide, and a video camera, which may be highly portable. Therefore, it is envisioned that the proposed method utilizing video-based vibrometry will be suitable for straightforward and reliable measurement of the liquid limit of cohesive soil in various applications and construction fields. The videos in this study are recorded at a rate of 250 frames per second. On the other hand, because the resonance frequency of soil samples converges to a small value close to zero as the liquid limit is approached, smartphones or webcam may even be suitable as the video camera for recording vibration signals in field applications since most modern smartphones provide camera recording capability of 30 frames per second (Marcu *et al*. 2020), 60 frames per second *(Marcu et al.* 2019), and even 120 frames per second (Marcu et al. 2018). Furthermore, a Raspberry Pi camera often employed for webcam provides 90 frames per second (Sands and Kim 2023).

4. Conclusions

In summary, this study investigates a novel method to characterize the liquid limit of cohesive soil by monitoring the vibration characteristics using a video camera. The key principle of this method is based on a hypothesis that the soil may lose elastic stability and thus its natural frequency

may approach zero as the water content level approaches the liquid limit. Impulsive base excitations are provided to kaolin clay samples by a simple and portable sliding platform devised in this study. Phase-based motion estimation technique is employed in this research to obtain the vibration characteristics of the soil samples by analyzing the optical flow in every pixel of the series of frames that effectively represents the motion of corresponding points of the soil specimen within the field of view of the camera. After computing a Fourier transform on the local phase signals extracted from the video and fitting the frequency spectrum around areas encompassing resonance to Lorentzian distribution, the liquid limit of cohesive soils may be readily identified by monitoring the resonance frequency that converges to zero as the water content level increases and approaches to the liquid limit. Thus, the proposed method yields a straightforward implementation that requires only a digital camera without the need for special equipment, which is not dependent on the proficiency of the operator as well. The experimental investigation results for various water content levels verify that the proposed method reliably and straightforwardly identifies the liquid limit of kaolin clay in a non-contact and non-destructive manner. Due to the nature of relatively soft soil near its liquid limit, the fundamental resonant frequency of the flexural mode may usually be low, allowing for video recordings to be taken at sampling rates that modern smartphones may easily reach. With smartphones seeing widespread use, especially as a form of communication in field environments, video-based vibrometery offers portable and reliable measurements from the commonly owned sensor. Thus, the proposed method yields great potential for a low-cost and portable method for determining the critical liquid limit of soil in field environments. Overall, the results of this study show promising potential of straightforwardly estimating the liquid limit of soil for a broad range of applications in practical field regardless of the operator's proficiency.

Acknowledgments

This research is supported by the faculty research seed grant from the College of Engineering and Computing at Georgia Southern University.

References

AASHTO (2013), "AASHTO T 89-13 standard method of test for determining the liquid limit of soils", *American Association of State and Highway Transportation Officials*.

Alrubaye Ali, J., Hasan, M. and Fattah Mohammed, Y. (2018), "Effects of using silica fume and lime in the treatment of kaolin soft clay", *Geomech. Eng.* **14**(3), 247-255. https://doi.org/10.12989/gae.2018.14.3.247.

ASTM (2000), "ASTM D2487-00 standard practice for classification of soils for engineering purposes (Unified soil classification system)", *ASTM International*. https://doi.org/10.1520/D2487-00.

ASTM (2005), "ASTM D4318 standard test method for liquid limit, plastic limit, and plasticity index of soils", *ASTM Int.*, https://doi.org/10.1520/D4318-05.

ASTM (2010), "ASTM D854-10 standard test methods for specific gravity of soil solids by water pycnometer", *ASTM Int*., https://doi.org/10.1520/D0854-10.

ASTM (2017), "ASTM D1140-17 standard test methods for determining the amount of material finer than 75-μm (No. 200) sieve in soils by washing", *ASTM Int.*, https://doi.org/10.1520/D1140-17.

Atterberg, A. (1911), "Die plastizitat der Tone", *Intern mitt. boden.*, 4-37.

Bore, T., Mishra, P.N., Wagner, N., Schwing, M., Honorio, T., Revil, A. and Scheuermann, A. (2021), "Coupled hydraulic, mechanical and dielectric investigations on kaolin", *Eng. Geol.*, **294**, 106352. https://doi.org/10.1016/j.enggeo.2021.106352.

British Standards Institute (2022), "Bs 1377-2:2022 methods of test for soils for civil engineering purposes – Part 2: classification tests and determination of geotechnical properties".

Çakar, E. and Yukselen-Aksoy, Y. (2021), "Ageing effect on compressibility, permeability and shear strength of clayey soils exposed to salt solutions", *Geomech. Eng.*, **25**(3), 245-251. https://doi.org/10.12989/gae.2021.25.3.245.

Casagrande, A. (1932). "Research on the Atterberg limits of soils." *Public Roads*, **13**(8), 121-130, 136.

Casagrande, A. (1958), "Notes on the design of the liquid limit device", *Géotechnique*, **8**(2), 84-91. https://doi.org/10.1680/geot.1958.8.2.84.

Chen, J.G., Wadhwa, N., Cha, Y.J., Durand, F., Freeman, W.T. and Buyukozturk, O. (2015), "Modal identification of simple structures with high-speed video using motion magnification", *J. Sound Vib.*, **345**, 58-71. https://doi.org/10.1016/j.jsv.2015.01.024.

Coduto, D., Yeung, M.C. and Kitch, W. (2011), *Geotechnical Engineering: Principles and Practices*.

Di Matteo, L. (2012). "Liquid limit of low- to medium-plasticity soils: Comparison between casagrande cup and cone penetrometer test", *Bull. Eng. Geol. Environ.*, **71**(1), 79-85. https://doi.org/10.1007/s10064-011-0412-5.

ISO (2022), "ISO 17892-12:2018/Amd 2:2022 geotechnical investigation and testing — laboratory testing of soil — Part 12: Determination of liquid and plastic limits — amendment 2".

Kim, J., Sapp, L. and Sands, M. (2022), "Simultaneous and contactless characterization of the Young's and shear moduli of gelatin-based hydrogels", *Exp. Mech.*, **62**. https://doi.org/10.1007/s11340-022-00891-1.

Knadel, M., Ur Rehman, H., Pouladi, N., Wollesen de Jonge, L., Moldrup, P. and Arthur, E. (2021), "Estimating atterberg limits of soils from reflectance spectroscopy and pedotransfer functions", *Geoderma*, **402**, 115300. https://doi.org/10.1016/j.geoderma.2021.115300.

Lee, J. and Shang, J. (2011), "Influencing factors on electrical conductivity of compacted kaolin clay", *Geomech. Eng.*, **3**(2), 131-151. https://doi.org/10.12989/gae.2011.3.2.131.

Lu, N. (2019), "Linking soil water adsorption to geotechnical engineering properties", *Geotechnical Fundamentals for Addressing New World Challenges*.

Marcu, A.E., Dobre, R.A., Datcu, O., Suciu, G. and Oh, J. (2019), "Flicker free VLC system with automatic code resynchronization using low frame rate camera", *Proceedings of the 2019 42nd International Conference on Telecommunications and Signal Processing (TSP.*

Marcu, A.E., Dobre, R.A. and Vlădescu, M. (2018), "Flicker free visible light communication using low frame rate camera", *Proceedings of the 2018 International Symposium on Fundamentals of Electrical Engineering (ISFEE)*.

Marcu, A.E., Dobre, R.A. and Vlădescu, M. (2020), "Flicker free optical camera communication for cameras capturing 30 frames

per second", *Proceedings of the 2020 43rd International Conference on Telecommunications and Signal Processing (TSP.*

Polidori, E. (2007), "Relationship between the atterberg limits and clay content", *Soils Found.*, **47**(5), 887-896. https://doi.org/10.3208/sandf.47.887.

Rehman, H. U., Knadel, M., Kayabali, K. and Arthur, E. (2019), "Estimating atterberg limits of fine-grained soils by visible–near-infrared spectroscopy", *Vadose Zone J.*, **18**(1), 190039. https://doi.org/10.2136/vzj2019.04.0039.

Sands, M. and Kim, J. (2023), " A low-cost and open-source measurement system to determine the Young's and shear moduli and poisson's ratio of soft materials using a raspberry Pi camera module and 3D printed parts", *HardwareX,* **13**, e00386. https://doi.org/10.1016/j.ohx.2022.e00386.

Shimobe, S. and Spagnoli, G. (2019), "A global database considering atterberg limits with the casagrande and fall-cone tests", *Eng. Geol.*, **260**, 105201. https://doi.org/10.1016/j.enggeo.2019.105201.

Simoncelli, E.P. and Freeman, W.T. (1995), "The steerable pyramid: A flexible architecture for multi-scale derivative computation", *Proceedings of the International Conference on Image Processing*.

Wadhwa, N., Rubinstein, M., Durand, F. and Freeman, W. (2013), "Phase-based video motion processing", Association for Computing Machinery (*ACM) Transactions on Graphics (TOG)*, **32**. https://doi.org/10.1145/2461912.2461966.

Yasodian, S., Dutta, R.K. and Seena, L. (2012), "Effect of microorganism on engineering properties of cohesive soils", *Geomech. Eng.*, **4**(2), 135-150. https://doi.org/10.12989/gae.2012.4.2.135.

Appendix

Table A1. Filter coefficients to compute horizontal and vertical local phase and local amplitude.

Tap #	G_{f1}	G_{f2}	H_{f1}	H_{f1}
-4	0.0094	0.0008	-0.0098	0.0008
-3	0.1148	0.0176	-0.0618	0.0176
-2	0.3964	0.1660	0.0998	0.1660
-1	-0.0601	0.6383	0.7551	0.6383
0	-0.9213	1.0000	0.0000	1.0000
1	-9.0601	0.6383	-0.7551	0.6383
2	0.3964	0.1660	-0.0998	0.1660
3	0.1148	0.0480	0.0618	0.0176
4	0.0094	0.0008	0.0098	0.0008

G_{f1} and G_{f2} indicate the horizontal and vertical phase filters for real horizontal ($G_2^{0^\circ}$) filter, respectively. H_{f1} and H_{f2} respectively indicate the horizontal and vertical phase filters for imaginary horizontal ($H_2^{0^\circ}$) filter. On the other hand, the real ($G_2^{90^\circ}$) and imaginary ($H_2^{90^\circ}$) vertical filters have the horizontal and vertical phase filters opposite to the real and imaginary horizontal filters. G_{f2} and G_{f1} are the horizontal and vertical phase filters for real vertical ($G_2^{90^\circ}$) filter, respectively. H_{f2} and H_{f1} respectively are the horizontal and vertical phase filters for imaginary vertical ($H_2^{90^\circ}$) filter.